ACS APPLIED MATERIALS & INTERFACES

Research Article

www.acsami.org

WO_3 Nanoparticle-Based Conformable pH Sensor

Lídia Santos,*[,§,⊥] Joana P. Neto,[§,⊥] Ana Crespo,[⊥] Daniela Nunes,[⊥] Nuno Costa,[†] Isabel M. Fonseca,[†] Pedro Barquinha,[⊥] Luís Pereira,[⊥] Jorge Silva,[‡] Rodrigo Martins,[⊥] and Elvira Fortunato*[,⊥]

[⊥]Departamento de Ciência dos Materiais, CENIMAT/I3N and CEMOP/Uninova, [†]REQUIMTE, and [‡]Departamento de Física, CEFITEC, Faculdade de Ciências e Tecnologia−Universidade Nova de Lisboa, 2829-516 Caparica, Portugal

Supporting Information

ABSTRACT: pH is a vital physiological parameter that can be used for disease diagnosis and treatment as well as in monitoring other biological processes. Metal/metal oxide based pH sensors have several advantages regarding their reliability, miniaturization, and cost-effectiveness, which are critical characteristics for in vivo applications. In this work, WO_3 nanoparticles were electrodeposited on flexible substrates over metal electrodes with a sensing area of 1 mm^2. These sensors show a sensitivity of −56.7 ± 1.3 mV/pH, in a wide pH range of 9 to 5. A proof of concept is also demonstrated using a flexible reference electrode in solid electrolyte with a curved surface. A good balance between the performance parameters (sensitivity), the production costs, and simplicity of the sensors was accomplished, as required for wearable biomedical devices.

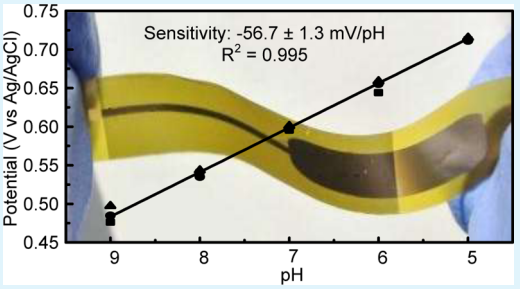

KEYWORDS: *pH sensor, tungsten oxide nanoparticles, hydrothermal synthesis, electrodeposition, flexible, lightweight*

INTRODUCTION

Cost-effective, flexible, lightweight, easy-to-fabricate, biocompatible, and wearable biomedical devices have recently attracted the focus of many research groups. The application of these devices is of extreme importance both in early diagnosis through continuous monitoring of complex health conditions and in patients under treatment.[1,2]

The pH value can be used as an indicator for disease diagnostics, medical treatment optimization, and monitoring of biochemical and biological processes.[3] Nevertheless, the integration of pH sensing systems into the next generation of wearable devices requires a different architecture than currently used in typical glass-type electrodes and a minimal electrode size.[4] Flexible pH sensors have already been reported on paper substrates, silicon nitride membranes, and polyimide substrates; however, full conformation with nonplanar surfaces, mechanical strain resistance, and miniaturization are still challenges to overcome.[5−7]

Ion sensitive field-effect transistors (ISFET), optical fiber, hydrogel films, and solid state pH sensors have been widely studied and reported for pH sensing.[8−13] Nevertheless, the power consumption, architecture, and cost of the sensors are a drawback. Metal oxide based sensing electrodes present several advantages due to their low manufacture costs, compatibility with miniaturization processes, high sensitivity, and abundancy.[14,15] Moreover, pH sensing can be achieved through a potentiometric method that is one of the most common, simple, and portable electrochemical techniques.[16]

Among the oxide materials being studied (IrO_x, RuO_2, SnO_2, Ta_2O_5, TiO_2, ZnO),[6,7,12,17−19] tungsten oxide (WO_3) is a very promising material regarding its low cost and availability, improved stability, good morphological and structural control of the synthesized nanostructures, reversible change of conductivity, high sensitivity, selectivity, and biocompatibility.[20] Furthermore, WO_3 is a well-studied wide band gap semiconductor (~2.75 eV) used for several applications as chromogenic material, sensing material, and catalyst.[21]

The first report of a WO_3 based pH sensor was published in 1987 by Wrighton et al.,[22] where a microelectrochemical transistor was operating either electrically or chemically by changing the gate voltage or the pH of the solution, respectively (Figure 1). Nevertheless, the use of WO_3 with high surface area was mainly reported for gas sensor applications and has not been fully exploited as pH sensing layer.[23,24]

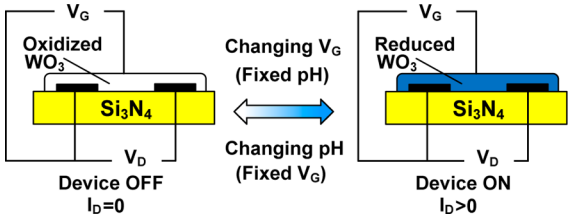

Figure 1. Simplified schematics of the first pH device using a WO_3 sensing layer. The device turns ON ($I_D > 0$) and OFF ($I_D = 0$) depending on the oxidized (insulating) or reduced (conductive) states of WO_3, respectively. A similar effect is observed by varying the pH (adapted from the work published by Wrighton et al.[22]).

Received: March 21, 2014
Accepted: July 14, 2014
Published: July 14, 2014

In this work, WO_3 based pH sensors with a reduced sensing area of 1 mm^2 were produced by electrodeposition of the nanoparticles previously grown by hydrothermal synthesis. This method allowed the production of a thin WO_3 layer with improved surface area and showed good sensitivity and stable response in a pH range between 9 and 5, which is in accordance with most physiological fluids.

For the first time (to the authors' knowledge), wax printing was used to produce the insulator layer in the pH sensors. This material is compatible with solution techniques and therefore is a good alternative for the conventional materials (polymers, photoresist or oxides) that usually require an additional step of patterning and/or are deposited by physical and expensive routes.

The polyimide substrate allowed a good conformation of the electrodes to curved surfaces thus making these suitable for applications in wearable biomedical devices.

EXPERIMENTAL SECTION

Hydrothermal Synthesis of Nanostructured WO_3. The chemicals used were of analytical grade without further purification. For the hydrothermal synthesis of WO_3 nanoparticles, 0.4 g of $Na_2WO_4{\cdot}2H_2O$ (Fluka, 99%) were first dissolved in 8 g of deionized water with 0.15 g of NaCl (Panreac, 99.5%) (as structure directing agent)[25] and then acidified with 1 g of 6 M HCl solution (Fluka, 37%). The final solution was transferred to a 23 mL PTFE chamber, set inside a stainless steel autoclave (4745 general purpose vessel, Parr) and installed in a oven (L3/11/B170, Nabertherm). The synthesis conditions were set at 180 °C for 1 h followed by a cooling period to room temperature inside the oven. The synthesis product was collected by centrifugation at 3000 rpm for 2 min (F140, Focus instruments) and washed three times with water. The final powder was finally dried in the oven (TK4067, EHRET) at 60 °C for at least 8 h.

WO_3 Characterization. Morphological and structural characterization of the powder was performed by scanning electron microscopy (SEM, Auriga SEM-FIB, Zeiss), X-ray diffraction (XRD, XPert PRO, PANalytical), and Fourier transform infrared spectroscopy (FTIR, Nicolet 6700, Thermo Electron Corporation). The nitrogen adsorption isotherm was obtained at 77 K in adsorption apparatus (ASAP 2010 Micromeritics) and the samples were degasified at 150 °C overnight. Hydrodynamic diameter of the WO_3 nanoparticles in water was confirmed by a dynamic light scattering (DLS) technique (W130i Avid Nano).

Sensor Fabrication. The fabrication of the sensor was executed in several steps as illustrated in Figure 2a. The polyimide film (50 μm thickness, DuPont) was cleaned by sonication (Bandelin Sonorex) in ethanol and isopropanol for 5 min and then dried under nitrogen flow before use. The mask used for patterning the electrode was made in acetate foil and defined with a laser cutter (Universal Laser System ULS3.50). A thin titanium layer (6 nm) was first deposited, by e-beam evaporation, in order to improve adhesion of the 65 nm gold layer. The delimitation of the sensing area (1 mm^2) was achieved by a wax printed layer (Xerox ColorQube 8570DNPS) on top of the connection line, which also worked as an insulator layer. The electrodeposition of WO_3 (Figure S1 from the Supporting Information) was performed using a Gamry Instruments Reference 600 potentiostat/galvanostat in a constant current mode (20 μA) for 900 s in a three electrode configuration. A Ag/AgCl reference electrode, a platinum wire

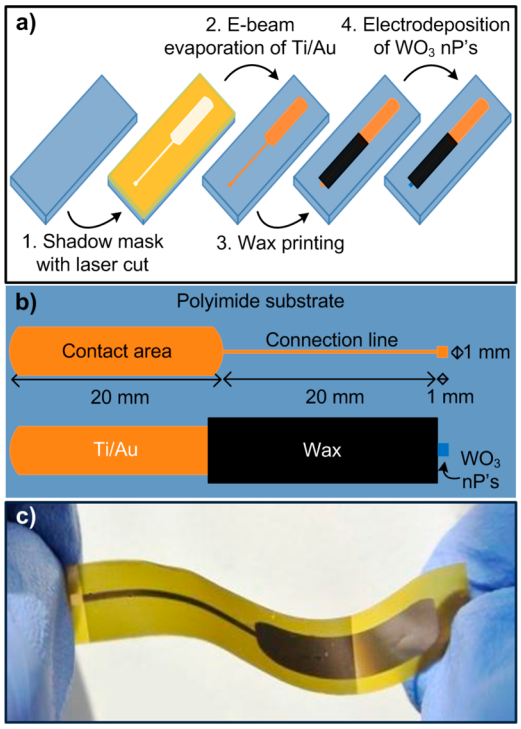

Figure 2. Scheme of the (a) sensor production procedure, (b) sensor design and structure, and (c) photograph of the final fabricated sensor.

counter electrode, and a gold layer, acting as the working electrode, were used to define the sensing layer of the pH sensor. A stable WO_3 nanoparticle dispersion in water (1 mg/mL) was achieved after magnetically stirring for 45 min and sonication (HIELSHER M80) for 5 min, followed by filtration (Sartorius, 0.45 μm pore diameter). After WO_3 nanoparticles deposition, the electrodes were rinsed with deionized water and dried for 1 h at 50 °C. The dimensions and macroscopic aspect of the final sensor are shown in Figure 2b and c. After deposition the homogeneity of the WO_3 sensing layer was confirmed by SEM analysis. For the focused ion beam (FIB) experiments, the WO_3 nanoparticles were previously coated with a carbon sacrificial layer, Ga^+ ions were accelerated to 30 kV at 2 pA and the etching depth was kept around 200 nm. The adhesion of the nanoparticles was checked by dipping the electrode in phosphate buffer solution (PBS, 5 mM, pH 7) at 37 °C for 8 days and measuring the amount of nanoparticles released into the solution by UV−vis spectroscopy (Spectro-115U, Gamry Instruments). A previous calibration was performed with WO_3 dispersions in PBS with different concentrations. After this test the sensor was again analyzed by SEM.

Sensor Cytocompatibility. Cytocompatibility of the sensor was evaluated according to the International Standard (ISO 10993-5) using the extract method. Three combinations of the materials used in the sensor production were tested: (1) polyimide substrate with gold electrode; (2) polyimide, gold, and wax layer; (3) the whole sensor (polyimide, gold, wax, and WO_3). For each material combination, three specimens were cut in small pieces and put inside a centrifuge tube. Three milliliters of complete culture medium (DMEM supplemented with 10% FBS and 1% penicillin−streptomycin, all from Invitrogen) were added to each tube. The tubes were placed inside an incubator at 37 °C for 48 h. All procedures involving the manipulation of cells or culture medium were performed

under aseptic conditions inside a biological safety cabinet (ESCO Labculture II). Vero cells were seeded at a density of 5 k cells per well in a 96 well microplate (Sarstedt) and were incubated at 37 °C in a 5% CO_2 humidified atmosphere incubator (Sanyo MCO19-AIC-UV). After 24 h, the medium was removed and 100 μL of conditioned medium was added to each well. Four replicas were prepared for each material and time point. Adequate controls—a positive control where 10 μL of DMSO was added to each well and a negative control—were also prepared. After 24, 48, and 72 h of incubation of the cells with the extracts, 10 μL of the cell viability indicator resazurin (0.25 mg/mL in PBS, Alfa Aesar) was added to each well and the cells were incubated two more hours in the CO_2 incubator. Absorbance of the medium was measured at 570 nm with a reference wavelength of 600 nm (Biotex ELX 800UV microplate reader). The absorbance of no cell control wells, containing only complete medium and the resazurin solution was also measured. The relative cell viability was calculated from the ratio of absorbances measured for the experimental wells and the negative control wells.

pH Sensor Characterization. The electrochemical characterization was performed in a typical three electrodes cell configuration as described above. Electrochemical impedance spectroscopy (EIS) measurements were recorded in a frequency range of 1 to 10^6 Hz with an AC voltage of 10 mV. The pH sensitivity of the sensors was assessed by measuring the open circuit voltage variation when the sensors were immersed in commercial buffer solutions with a pH in the range of 5 to 9 (buffer solutions, Roth) for 120 s at room temperature.

Proof of Concept. For the proof of concept a flexible Ag/AgCl reference electrode was built using the same dimensions already described for the pH sensor. Thin layers of chromium (7 nm), platinum (3 nm), and silver (30 nm) were sequentially deposited by electron-beam evaporation (procedure based on the work of Huang et al.[6]). The AgCl layer was formed by anodization of the silver film applying a constant current at 0.5 mA in 0.1 M HCl for 5 s. The electrode was rinsed with water and saturated in 3 M KCl solution before use. The characterization of the electrode was performed by EIS in PBS. See Supporting Information Figure S2.

The solid electrolyte was prepared by dissolving gelatin (mass fraction of 8%) in commercial pH buffer solutions from Roth (pH 8, 7 and 6) at 50 °C. After complete dissolution, the solution was transferred to a recipient and cooled down in order to achieve the required curved conformation.

The electrochemical measurements shown in the proof of concept section were obtained using the pH sensor as working electrode and the flexible Ag/AgCl reference electrode, both in contact with the solid electrolyte.

RESULTS AND DISCUSSION

WO_3 Nanoparticle Characterization. Hydrothermal synthesis was the method chosen to prepare the nanoparticles due its low process temperature, easy control of the morphology and structure of the nanoparticles, and good reproducibility. In this work, WO_3 nanoparticles were obtained from a commercial precursor (sodium tungstate) with a structure directing agent (sodium chloride) that promotes uniformity of the nanoparticles size and shape thus improving the reliability of the sensing layer.

The morphology of the synthesized WO_3 nanoparticles was observed by SEM (Figure 3). The size of the nanoparticles was

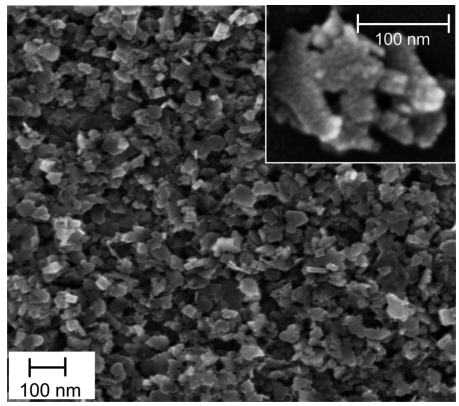

Figure 3. SEM image of WO_3 nanoparticles. The inset shows a higher magnification of the nanoparticles exhibiting nanoslab-type shape agglomerates.

estimated to be approximately 10 nm, resulting in nanoslab-type shape agglomerates. The mean hydrodynamic diameter of 75 nm determined by DLS for the nanoparticles dispersion in water is in accordance with the agglomerates sizes observed by SEM.

The WO_3 crystalline structure was verified by XRD (Figure 4a). The diffraction peaks are attributed to orthorhombic hydrated tungsten oxide (*ortho*-$WO_3{\cdot}0.33H_2O$), according to the reference pattern ICDD 01-072-0199, with a mixture of a secondary product (*) not yet identified. In the literature,[26] the particular peak at 10° was also found in WO_3 films deposited at low temperatures thus suggesting that the corresponding structure derives from the slow growing of the nanoparticles clusters. This is corroborated by the presence of broad peaks characteristic of small crystallite sizes and by the X-ray microanalysis that indicate the presence of only W and O elements in the sample (result not shown here), confirming that the nonidentified peaks do not arrise from any impurity.

Tungsten oxides follow a well-known[27] ReO_3-type structure built up of layers containing distorted corner-shared WO_6 octahedra. The obtained *ortho*-$WO_3{\cdot}0.33H_2O$ structure (represented in Figure 4b) includes two types of octahedra: one is formed by W−O covalent bonds and the other by two types of terminal bonds (W═O and W−OH). This structure will restrict the stacking along the *z* axis due to the weak interaction between adjacent layers thus preventing bulk type structures. The recorded FTIR spectra (Figure 4c) allowed the identification of both terminal groups and vibrations in WO_6 octahedron, which are in accordance to the state of the art.[28,29] The broad absorption band at 3485 cm^{-1} (−OH stretching) and sharp band at 1605 cm^{-1} (−OH in plane bending) indicates the presence of water molecules in the structure. The broad band between 570 and 970 cm^{-1} has been ascribed to the O−W−O stretching and bending modes and stretching of the W═O double bond.

The surface area characterization was performed employing the Brunauer−Emmet−Teller (BET) method and the resulting nitrogen adsorption−desorption isotherm (Figure 4d) demonstrates a typical type IV behavior indicative of the presence of mesopores. The pore size distribution is mainly attributed to narrow mesopores in the range of 10 nm with some micropores <2 nm. The hysteresis shape (H1 type) also suggests the presence of rigid agglomerates of uniform size with a narrow pore size distribution. This result confirms the previously described SEM images where the porosity is due to the

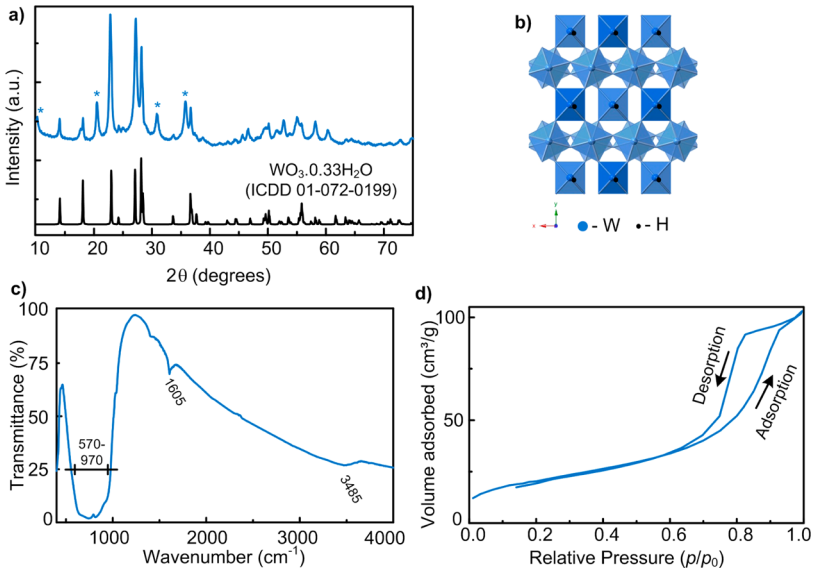

Figure 4. (a) XRD diffractograms of WO_3 synthesized powder and orthorhombic $WO_3{\cdot}0.33H_2O$ reference pattern (the * peaks correspond to unidentified structure). (b) Crystal structure simulation of orthorhombic $WO_3{\cdot}0.33H_2O$ (produced in crystal maker software). (c) FTIR spectrum and (d) nitrogen adsorption–desorption isotherms of WO_3 nanoparticles performed at standard temperature and pressure (STP).

agglomeration of small nanoparticles. The resulting active surface area (74 m^2/g) gives a good approximation of the real surface area of nanoparticles and is in accordance with previous studies.[30,31]

From all the characterization results, we can conclude that the synthesized WO_3 powder is formed by agglomerates of small nanoparticles with a mesoporous structure. The reduced nanoparticle size is an important feature for the enhancement of the sensor performance since it increases the surface area.[32]

Sensor Assembly. The pH sensor was produced using the sequence previously shown in Figure 2. First, the gold layer was deposited by e-beam evaporation on a polyimide substrate. Then the sensing area was delimited by wax printing and finally, WO_3 nanoparticles were electrodeposited applying a fixed current method. All the materials used in the sensor production (polyimide, gold, and WO_3) have already been proven to be biocompatible and adequate for biomedical devices. Nonetheless, the wax and the whole sensor cytocompatibility were tested in a conventional procedure, as explained below.

Wax Cytocompatibility. Resazurin is a redox dye, blue and nonfluorescent, that is reduced to resorufin, pink and fluorescent, by viable metabolically active cells. The rate of dye reduction is directly proportional to the number of viable cells present. Resorufin has an absorption maximum at 570 nm while resazurin peak absorption is at 600 nm. The results summarized in Table 1 show the relative cell viabilities obtained for the three material combinations, positive and negative controls. The relative cell viabilities are consistently above 90% for all experimental conditions and time points. We can conclude that none of the materials tested is cytotoxic, in particular the printed wax is not cytotoxic and can therefore be used as an insulator.

Table 1. Relative Cell Viabilities after 24, 48, and 72 h of Incubation of the Cells with Conditioned Media

sample	24 h	48 h	72 h
polyimide/Au	0.98 ± 0.04	1.00 ± 0.03	1.10 ± 0.05
polyimide/Au/wax	0.96 ± 0.03	1.00 ± 0.02	1.15 ± 0.08
polyimide/Au/wax/WO_3	1.01 ± 0.03	1.03 ± 0.02	1.20 ± 0.07
negative control	1.00 ± 0.02	1.00 ± 0.02	1.00 ± 0.05
positive control	0.03 ± 0.02	0.013 ± 0.002	0.012 ± 0.011

Sensing Layer. The electrodeposited WO_3 nanoparticles resulted in a uniform sensing layer with some small agglomerates, observed by SEM (Figure 5a). This image shows that even if the nanoparticles are agglomerated in nanoslabs in solution, after electrodeposition they can dissociate and produce a high quality thin layer with enhanced specific surface area. Milling with FIB (Figure 5b) allowed the determination of the sensing layer thickness in which is ~55 nm.

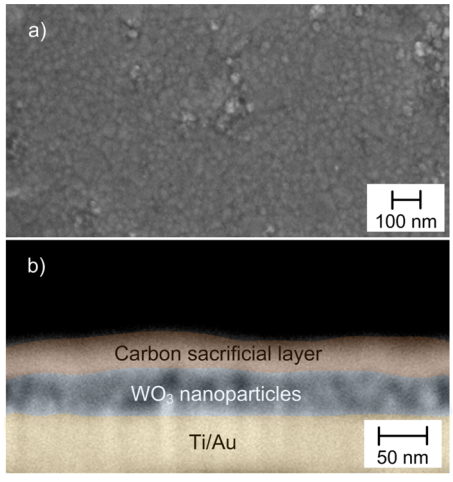

Figure 5. SEM images of (a) sensing area after $WO_3{\cdot}0.33H_2O$ nanoparticles electrodeposition; (b) cross-section overview of Ti/Au, electrodeposited WO_3 nanoparticles, and carbon sacrificial layers after FIB milling (The image was colored for better understanding of the layered structure).

The effective adhesion of the nanoparticles was tested by immersing the sensors in PBS solution at 37 °C for 8 days and measuring the UV–vis spectra of the solution during this

period. The transmittance was compared with the calibration curve obtained for different dispersions of WO_3 nanoparticles in PBS at 280 nm (Figure 6). After 8 days, the morphology of

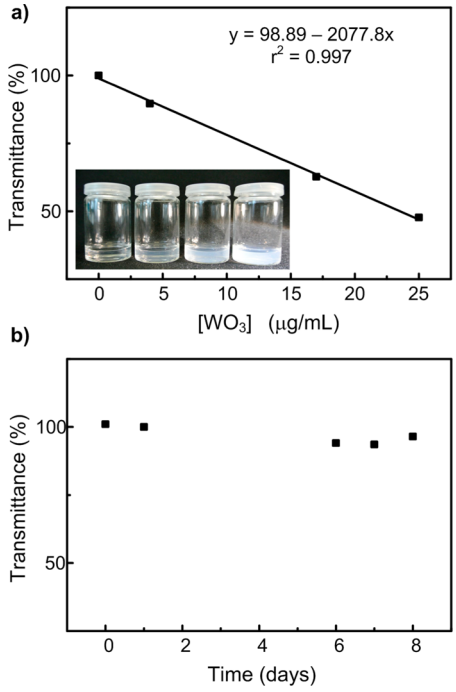

Figure 6. (a) Calibration curve of transmittance values at 280 nm wavelength for WO_3 dispersions of different concentrations. (b) Transmittance of the PBS solution after dipping the WO_3 sensor at 37 °C for 8 days.

the sensing area was analyzed by SEM (image not shown) and no significant change was noticed. The slight decrease in transmittance after the sixth day corresponds to a WO_3 mass fraction of 0.002% which represents a negligible deterioration of the sensing layer. Therefore, we can confirm a good adhesion of the nanoparticles after immersion for 1 week in PBS at 37 °C.

WO_3 Sensing Layer Electrochemical Characterization. The impedance modulus and phase angle of the electrode was analyzed before and after deposition of the WO_3 nanoparticles to evaluate the contribution of the coating to the overall charge transport characteristics at the electrode/solution interface (Figure 7). Both electrodes exhibit similar high-frequency

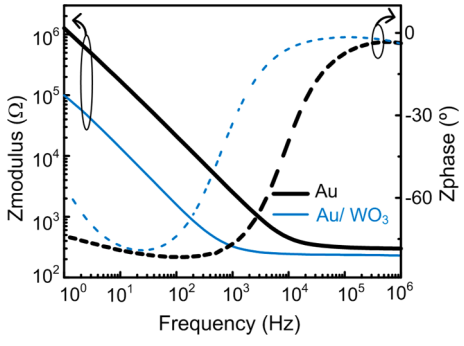

Figure 7. Impedance modulus (solid lines) and phase angle (dashed lines) plots of the electrode before and after $WO_3 \cdot 0.33H_2O$ nanoparticles electrodeposition.

impedance (10^4–10^6 Hz) and a near-resistive phase angle (approaching 0°) which is mainly determined by the contribution of the solution.[4] Nonetheless, the frequency range over which the phase value is near 0° increased by coating the electrode with WO_3 nanoparticles.

In the low-frequency range, the frequency dependent impedance and the phase angle near −90° indicates that the current flow is dominated by capacitive charging. The decrease of about 1 order of magnitude in the impedance after deposition of the nanoparticles is due to the increase of the electrochemical surface area and it clearly confirms that the deposited WO_3 layer will improve the sensitivity of the produced pH sensor.[4,33]

pH Sensitivity and Reproducibility. The pH sensitivity was confirmed by measuring the open circuit voltage when dipping the sensor in commercial buffer solutions for 120 s. The measurements were performed from pH 9 to pH 5 with three distinct sensors (Figure 8a).

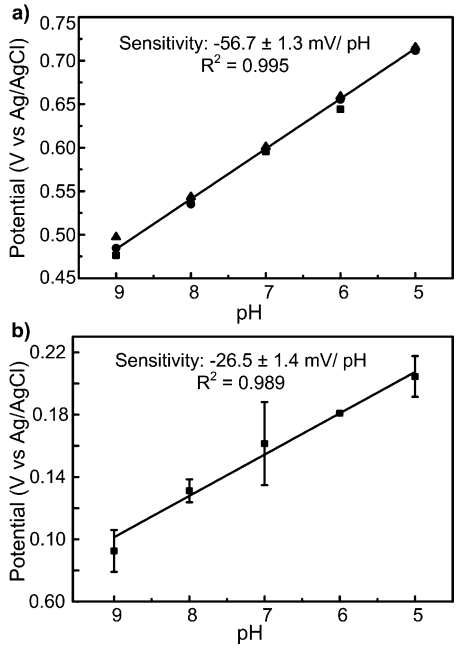

Figure 8. pH sensitivity measured from pH 9 to 5 of (a) Au/WO_3 nanoparticles electrodes and (b) Au electrode. The sensitivity is indicated inside the graphic.

The sensing mechanism for this material, even if not fully understood, is believed to be dependent on the redox reaction involving the double injection of cations and electrons to the structure, thus forming a tungsten oxide bronze with higher conductivity than tungsten oxide:

$$WO_3 + xe^- + xH^+ \leftrightarrow H_xWO_3 \quad (1)$$

x corresponds to the number of protons (H^+) and electrons (e^-) involved in the reaction and H_xWO_3 represents the tungsten bronze. The reaction mechanism is explained by means of small polaron transitions (formation of W^{5+} sites) for amorphous films and Drude-like free electron scattering for crystalline films. The major difference between these two mechanisms for amorphous and crystalline tungsten oxide films is the electron localization or delocalization.[34−36]

The measured potential is therefore dependent on the pH and if there is a linear relation between these two parameters

Table 2. Electrochemical Potential Values of Three WO_3 Sensors Measured from pH 9 to 5 and Corresponding Sensitivity

	sensor 1	sensor 2	sensor 3	mean potential
pH 9 (mV)	476	485	497	486 ± 11
pH 8 (mV)	541	535	544	540 ± 4
pH 7 (mV)	596	599	601	598 ± 3
pH 6 (mV)	644	655	659	653 ± 8
pH 5 (mV)	713	711	715	713 ± 2
pH sensitivity (mV/pH)[a]	−57.6 ± 1.8 (R^2 = 0.996)	−57.4 ± 1.0 (R^2 = 0.999)	−55.2 ± 1.3 (R^2 = 0.998)	−56.7 ± 1.1 (R^2 = 0.995)

[a]The uncertainty corresponds to the standard deviation of the linear regressions, and R^2 is the correlation coefficient.

then it is described to have a Nernstian behavior. The sensitivity of the sensor can, in that case, be obtained by the slope of the linear regression according to the equation:[3]

$$E = E^0 - (2.303RT/F)\text{pH} = E^0 - 0.05916\text{pH} \quad (2)$$

Where E^0 corresponds to the standard electrode potential, R is the gas constant, T is the temperature, and F is Faraday's constant. The resulting theoretical maximum sensitivity is −59 mV/pH. In this situation all space charges are formed, owing to the redox reaction, indicating a good performance of the sensor. The pH sensors produced in this work (Figure 8a) demonstrated a mean sensitivity value of −56.7 ± 1.3 mV/pH, which is very close to the maximum theoretical value. This confirms the good sensitivity of the WO_3 nanoparticles to the variation of proton's concentration in solution due to the redox reaction 1 involved in the process. The measured potential values of the three sensors in different pH solutions (Table 2) showed small standard deviation, between 2 and 11 mV, which indicates that the experimental method used to produce these pH sensors is stable and reproducible.

Two gold electrodes, without WO_3 nanoparticles, were also measured for comparison. The mean sensitivity decreased by 50% associated with a higher standard deviation in each point and a lower correlation coefficient of the linear fitting (Figure 8b). Therefore, we confirmed that the pH sensitivity is enhanced due to the presence of the WO_3 nanoparticles layer.

Reversibility. The same sensor was continuously tested in cycles from pH 9 to 5 (Figure 9). This procedure aims to simulate the in vivo conditions where the pH sensor will be exposed for long periods to oscillating pH levels. It is clear that the electrochemical potential varies with the pH level but the sensitivity is slightly dependent on the scanning direction (Table 3). The sensitivity decreased by 11.6% between the first and third cycle which we believe is related with reactions at the electrode surface and charge saturation sites that occurs during electrode aging.[3]

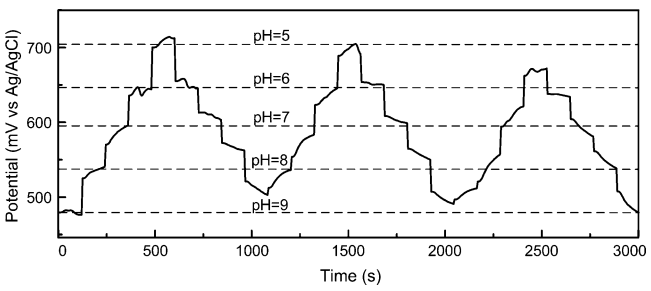

Figure 9. Electrochemical potential behavior of the pH sensor during three completes cycles for pH range of 9−5 and 5−9.

Further testing is being performed to evaluate the sensor sensitivity dependence on the WO_3 nanoparticles characteristics, such as active surface area and conductivity. Furthermore, the existence of two WO_3 crystallographic structures (Figure 4a) in the produced dispersion can also contribute to a faster degradation of the sensing layer. Nevertheless, the low hysteresis values, between 6 and 10 mV, obtained for all pH solutions are comparable with the literature[6,19] and confirms the sensor stability.

Response Time. The sensor's response time was measured for three buffer solutions of different pH. The potential was measured before and after dipping the WO_3 electrode in the buffer solutions for approximately 20 s (Figure 10). The response time was calculated as the time necessary to reach 90% of the maximum potential value, varying from 23 to 28 s in this pH range. These values are higher than those reported for other metal oxide electrodes,[37] which is attributed to differences in the structure of the sensor and in the experimental procedure. In our set up the electrode is kept in dry conditions before dipping in the solution therefore, the time to reach the equilibrium between the pH of solution and the electrode interface is higher than when the equilibrium is reached starting with the electrode already immersed in the electrolyte. The porosity of the sensing layer, when using WO_3 nanoparticles, is another factor that contributes to the increase of the time required to reach this equilibrium.[38] Nevertheless, the fact that this sensor can respond to pH variations in commercial buffer solutions, containing a complex mixture of different ions, allow us to conclude that this material has a good selectivity to protons.

Proof of Concept: Flexible pH Sensor. In order to prove the potential application of the produced WO_3 sensor in wearable biomedical devices, we developed a flexible reference electrode with the same size and substrate as the pH sensor. The electrochemical potentials were recorded for 120 s in a gelatin-based electrolyte with a curved surface (Figure 11).

The lower sensitivity of this preliminary test is attributed to the solid electrolyte, namely the low ion mobility and the use of commercial buffer solutions that contains a mixture of different ions, which difficult the occurrence of the redox reaction in the electrode surface. Further studies are required in order to evaluate all the limitations of this concept and improve ion mobility of the solid electrolyte. Nevertheless, the flexibility and conformability of the sensors to curved surfaces were proved to be effective and therefore adaptable to applications as wearable biomedical devices.

As a conclusion, the sensitivity of the WO_3 nanoparticles based pH sensor in aqueous electrolyte is comparable to that of other metal oxides nanoparticles, such as RuO_2,[39] ZnO nanotubes,[17] and IrO_x[6] with the advantage of solution

Table 3. Electrochemical Potential Values for the Same WO_3 Sensor Measured from pH 9 to 5 and 5 to 9, during Three Complete Cycles, and the Resulting Sensitivity

	cycle 1	cycle 2	cycle 3	mean potential
pH 9 (mV)	476	503	485 ± 4	488 ± 7
pH 8 (mV)	551 ± 7	543 ± 5	526 ± 9	540 ± 7
pH 7 (mV)	600 ± 3	591 ± 5	569 ± 8	587 ± 9
pH 6 (mV)	645 ± 1	648 ± 1	628 ± 4	640 ± 6
pH 5 (mV)	713	692	672	692 ± 10
pH sensitivity−pH 9 to 5[a] (mV/pH)	−57.6 ± 1.8 (R^2 = 0.996)	−48.7 ± 2.7 (R^2 = 0.987)	−47.2 ± 4.5 (R^2 = 0.965)	−50.9 ± 2.9
pH sensitivity−pH 5 to 9[a] (mV/pH)	−50.3 ± 2.6 (R^2 = 0.990)	−50.2 ± 1.7 (R^2 = 0.996)	−48.3 ± 2.0 (R^2 = 0.993)	−49.6 ± 0.7

[a]The uncertainty corresponds to the standard deviation of the linear regressions, and R^2 is the correlation coefficient.

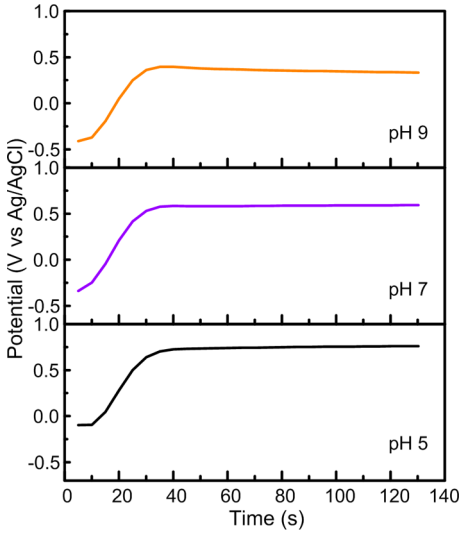

Figure 10. Electrochemical potential behavior of the electrode after dipping in buffer solution of pH 9, 7, and 5. The response time was calculated as the time necessary to reach 90% of the maximum potential value.

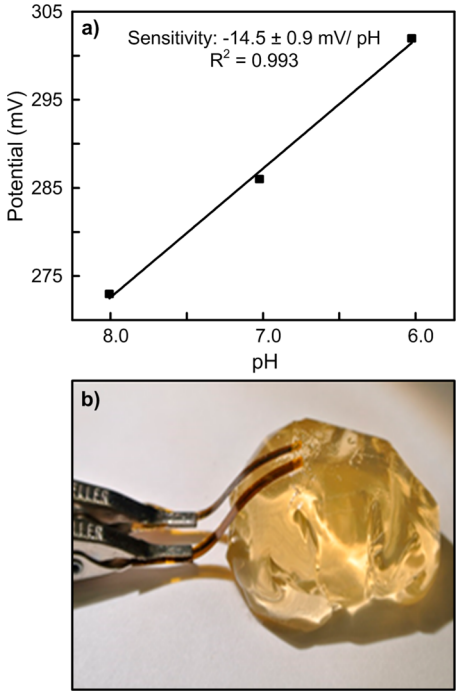

Figure 11. (a) pH sensitivity of WO_3 sensor using a flexible Ag/AgCl reference electrode in a nonplanar surface made of gelatin-based electrolyte. (b) Photograph of the prototype.

processing, low temperature, and facile manufacture, being adaptable to different sensor architectures.

CONCLUSIONS

Flexible sensors based on WO_3 nanoparticles with a high surface area were produced by electrodeposition on gold electrodes with a sensing area of 1 mm^2. The wax printed layer, here used as an insulator, was proven to be cytocompatible and therefore, a good alternative for sensor assembly. The pH sensitivity of these electrodes shows a near-Nernstain response of −56.7 ± 1.3 mV/pH and reversibility was confirmed for three complete cycles in a pH range of 9−5.

The application of WO_3 flexible sensors to curved surfaces with a flexible Ag/AgCl reference electrode and solid electrolyte, shows a linear response in the pH range from 8 to 6, with a sensitivity of 14.5 mV/pH but with good possibilities of improvement, for instance, by optimizing the solid electrolyte and assembly processes.

As a conclusion, these results show that WO_3 nanoparticles are a promising material for the development of stable and flexible pH sensors with low cost fabrication processes, low power consumption, and small size that can be integrated in biomedical flexible devices without the need for bulky glass reference electrodes. Furthermore, this type of sensor can also be adapted to other applications in a variety of fields such as food packaging, soil monitoring in agriculture, erosion monitoring in construction, or even lubricants.

ASSOCIATED CONTENT

Supporting Information

Electrodeposition setup and electrochemical impedance spectroscopy of Ag/AgCl flexible reference electrode. This material is available free of charge via the Internet at http://pubs.acs.org.

AUTHOR INFORMATION

Corresponding Authors

*E-mail: ls.santos@campus.fct.unl.pt (L.S.).
*E-mail: emf@fct.unl.pt (E.F.).

Author Contributions

[§]These authors contributed equally. The manuscript was written through contributions of all authors. All authors have given approval to the final version of the manuscript.

Notes

The authors declare no competing financial interest.

■ ACKNOWLEDGMENTS

This work was funded by the Portuguese Science Foundation (FCT-MEC) through project EXCL/CTM-NAN/0201/2012, Strategic Project PEst-C/CTM/LA0025/2013-14, and the FCT-MCTES doctoral grants SFRH/BD/73810/2010 given to L.S. and SFRH/BD/76004/2011 given to J.N. Moreover, this work was also supported by E.F.'s ERC 2008 Advanced Grant (INVISIBLE contract number 228144).

■ REFERENCES

(1) Pang, C.; Lee, C.; Suh, K.-Y. Recent Advances in Flexible Sensors for Wearable and Implantable Devices. *J. Appl. Polym. Sci.* **2013**, *130*, 1429−1441.
(2) Segev-Bar, M.; Haick, H. Flexible Sensors Based on Nanoparticles. *ACS Nano* **2013**, *7*, 8366−8378.
(3) Zhou, D. D. Microelectrodes for in-Vivo Determination of pH. In *Electrochemical sensors, biosensors and their biomedical applications*; Academic Press, Inc., 2008; pp 261−305.
(4) Shanmugasundaram, B.; Gluckman, B. J. Micro-Reaction Chamber Electrodes for Neural Stimulation and Recording*Conference Proceedings of the 33rd Annual International Conference of the IEEE Engineering in Medicine and Biological Society,* Boston, MA, Aug 30−Sep 3, 2011; pp 656−659.
(5) Bandodkar, A. J.; Hung, V. W. S.; Jia, W.; Valdés-Ramírez, G.; Windmiller, J. R.; Martinez, A. G.; Ramírez, J.; Chan, G.; Kerman, K.; Wang, J. Tattoo-Based Potentiometric Ion-Selective Sensors for Epidermal pH Monitoring. *Analyst* **2013**, *138*, 123−128.
(6) Huang, W.-D.; Cao, H.; Deb, S.; Chiao, M.; Chiao, J. C. A Flexible pH Sensor Based on the Iridium Oxide Sensing Film. *Sensors Actuators A Phys.* **2011**, *169*, 1−11.
(7) Kuo, L.-M.; Chen, K.-N.; Chuang, Y.-L.; Chao, S. A Flexible pH-Sensing Structure Using WO3/IrO2 Junction with Al2O3 Encapsulation Layer. *ECS Solid State Lett.* **2013**, *2*, P28−P30.
(8) Gerlach, G.; Guenther, M.; Sorber, J.; Suchaneck, G.; Arndt, K.-F.; Richter, A. Chemical and pH Sensors Based on the Swelling Behavior of Hydrogels. *Sensors Actuators B Chem.* **2005**, *111−112*, 555−561.
(9) Kinlen, P. J.; Heider, J. E.; Hubbard, D. E. A Solid-State pH Sensor Based on a Nafion-Coated Iridium Oxide Indicator Electrode and a Polymer-Based Silver Chloride Reference Electrode. *Sensors Actuators B Chem.* **1994**, *22*, 13−25.
(10) Pinto, J. V.; Branquinho, R.; Barquinha, P.; Alves, E.; Martins, R.; Fortunato, E. Extended-Gate ISFETs Based on Sputtered Amorphous Oxides. *J. Dispersion Technol.* **2013**, *9*, 729−734.
(11) Safavi, A.; Bagheri, M. Novel Optical pH Sensor for High and Low pH Values. *Sensors Actuators B Chem.* **2003**, *90*, 143−150.
(12) Branquinho, R.; Pinto, J. V.; Busani, T.; Barquinha, P.; Pereira, L.; Baptista, P. V.; Martins, R.; Fortunato, E. Plastic Compatible Sputtered Ta2O5 Sensitive Layer for Oxide Semiconductor TFT Sensors. *J. Dispersion Technol.* **2013**, *9*, 723−728.
(13) Wang, X.-D.; Wolfbeis, O. S. Fiber-Optic Chemical Sensors and Biosensors (2008−2012). *Anal. Chem.* **2013**, *85*, 487−508.
(14) Zeng, J.; Hu, M.; Wang, W.; Chen, H.; Qin, Y. NO2-Sensing Properties of Porous WO3 Gas Sensor Based on Anodized Sputtered Tungsten Thin Film. *Sensors Actuators B Chem.* **2012**, *161*, 447−452.
(15) Barquinha, P.; Martins, R.; Pereira, L.; Fortunato, E. *Transparent Oxide Electronics*; John Wiley & Sons, Ltd, 2012.
(16) Bakker, E.; Pretsch, E. Modern Potentiometry. *Angew. Chem.* **2007**, *46*, 5660−5668.
(17) Fulati, A.; Ali, S. M. U.; Riaz, M.; Amin, G.; Nur, O.; Willander, M. Miniaturized pH Sensors Based on Zinc Oxide Nanotubes/Nanorods. *Sensors* **2009**, *9*, 8911−8923.
(18) Vieira, N. C. S.; Figueiredo, A.; Faceto, A. D.; de Queiroz, A. A. A.; Zucolotto, V.; Guimarães, F. E. G. Dendrimers/TiO2 Nanoparticles Layer-by-Layer Films as Extended Gate FET for pH Detection. *Sensors Actuators B Chem.* **2012**, *169*, 397−400.
(19) Kurzweil, P. Metal Oxides and Ion-Exchanging Surfaces as pH Sensors in Liquids: State-of-the-Art and Outlook. *Sensors* **2009**, *9*, 4955−4985.
(20) Yuan, S.-J.; He, H.; Sheng, G.-P.; Chen, J.-J.; Tong, Z.-H.; Cheng, Y.-Y.; Li, W.-W.; Lin, Z.-Q.; Zhang, F.; Yu, H.-Q. A Photometric High-Throughput Method for Identification of Electrochemically Active Bacteria Using a WO3 Nanocluster Probe. *Sci. Rep.* **2013**, *3*, 1315.
(21) Vernardou, D.; Drosos, H.; Spanakis, E.; Koudoumas, E.; Savvakis, C.; Katsarakis, N. Electrochemical and Photocatalytic Properties of WO3 Coatings Grown at Low Temperatures. *J. Mater. Chem.* **2011**, *21*, 513.
(22) Natan, M. J.; Mallouk, T. E.; Wrighton, M. S. pH-Sensitive WO3-Based Microelectrochemical Transistors. *J. Phys. Chem.* **1987**, *91*, 648−654.
(23) Choi, Y.-G.; Sakai, G.; Shimanoe, K.; Yamazoe, N. Wet Process-Based Fabrication of WO3 Thin Film for NO2 Detection. *Sensors Actuators B Chem.* **2004**, *101*, 107−111.
(24) Heidari, E. K.; Zamani, C.; Marzbanrad, E.; Raissi, B.; Nazarpour, S. WO3-Based NO2 Sensors Fabricated through Low Frequency AC Electrophoretic Deposition. *Sensors Actuators B Chem.* **2010**, *146*, 165−170.
(25) Wang, J.; Khoo, E.; Lee, P. S.; Ma, J. Synthesis, Assembly, and Electrochromic Properties of Uniform Crystalline WO3 Nanorods. *J. Phys. Chem. C* **2008**, *112*, 14306−14312.
(26) Deepa, M.; Kar, M.; Agnihotry, S. A. Electrodeposited Tungsten Oxide Films: Annealing Effects on Structure and Electrochromic Performance. *Thin Solid Films* **2004**, *468*, 32−42.
(27) Yang, J.; Jiao, L.; Zhao, Q.; Wang, Q.; Gao, H.; Huan, Q.; Zheng, W.; Wang, Y.; Yuan, H. Facile Preparation and Electrochemical Properties of Hierarchical Chrysanthemum-like WO3·0.33H2O. *J. Mater. Chem.* **2012**, *22*, 3699.
(28) Yayapao, O.; Thongtem, T.; Phuruangrat, A.; Thongtem, S. CTAB-Assisted Hydrothermal Synthesis of Tungsten Oxide Microflowers. *J. Alloys Compd.* **2011**, *509*, 2294−2299.
(29) Deepa, M.; Sharma, N.; Varshney, P.; Varma, S. P.; Agnihotry, S. A. FTIR Investigations of Solid Precursor Materials for Sol-Gel Deposition of WO3 Based Electrochromic Films. *J. Mater. Sci.* **2000**, *35*, 5313−5318.
(30) Lu, Z.; Kanan, S. M.; Tripp, C. P. Synthesis of High Surface Area Monoclinic WO3 Particles Using Organic Ligands and Emulsion Based Methods. *J. Mater. Chem.* **2002**, *12*, 983−989.
(31) Gu, Z.; Li, H.; Zhai, T.; Yang, W.; Xia, Y.; Ma, Y.; Yao, J. Large-Scale Synthesis of Single-Crystal Hexagonal Tungsten Trioxide Nanowires and Electrochemical Lithium Intercalation into the Nanocrystals. *J. Solid State Chem.* **2007**, *180*, 98−105.
(32) Vemuri, R. S.; Bharathi, K. K.; Gullapalli, S. K.; Ramana, C. V. Effect of Structure and Size on the Electrical Properties of Nanocrystalline WO3 Films. *ACS Appl. Mater. Interfaces* **2010**, *2*, 2623−2628.
(33) Weiland, J. D.; Anderson, D. J.; Humayun, M. S. In Vitro Electrical Properties for Iridium Oxide versus Titanium Nitride Stimulating Electrodes. *IEEE Trans. Biomed. Eng.* **2002**, *49*, 1574−1579.
(34) Lee, S.-H.; Je, M.; Cheong, H. M.; Ozkan, E.; Tracy, E. C.; Deb, S. K. Effect of Crystallinity on Electrochromic Mechanism of LixWO3 Thin Films. *Solid State Ionics* **2003**, *156*, 447−452.
(35) Lampert, C. M. Electrochromic Materials and Devices for Energy Efficient Windows. *Sol. Energy Mater.* **1984**, *11*, 1−27.
(36) Hotchandani, S.; Bedja, I.; Fessenden, R.; Kamat, P. Electrochromic and Photoelectrochromic Behavior of Thin WO3 Films Prepared from Quantum Size Colloidal Particles. *Langmuir* **1994**, *10*, 17−22.
(37) Da Silva, G. M.; Lemos, S. G.; Pocrifka, L. A.; Marreto, P. D.; Rosario, A. V.; Pereira, E. C. Development of Low-Cost Metal Oxide pH Electrodes Based on the Polymeric Precursor Method. *Anal. Chim. Acta* **2008**, *616*, 36−41.

(38) Olthuis, W.; Robben, M. A. M.; Bergveld, P.; Bos, M.; Van der Linden, W. E. pH Sensor Properties of Electrochemically Grown Iridium Oxide. *Sensors Actuators B Chem.* **1990**, *2*, 247−256.
(39) Maurya, D. K.; Sardarinejad, A.; Alameh, K. High-Sensitivity pH Sensor Employing a Sub-Micron Ruthenium Oxide Thin-Film in Conjunction with a Thick Reference Electrode. *Sensors Actuators A Phys.* **2013**, *203*, 300−303.